CHIN. PHYS. LETT. Vol. 34, No. 4 (2017) 047302

Magnetic Transport Properties of Fe-Phthalocyanine Dimer with Carbon Nanotube Electrodes *

Yu-Zhuo Lv(吕钰卓)[1], Peng Zhao(赵朋)[1**], De-Sheng Liu(刘德胜)[2,3]

[1]School of Physics and Technology, University of Jinan, Jinan 250022
[2]School of Physics, Shandong University, Jinan 250100
[3]Department of Physics, Jining University, Qufu 273155

(Received 4 December 2016)

Based on the non-equilibrium Green's method and density functional theory, the magnetic transport of Fe-phthalocyanine dimers with two armchair single-walled carbon nanotube electrodes is investigated. The results show that the system can present high-performance spin filtering, magnetoresistance, and low-bias spin negative differential resistance effects by tuning the external magnetic field. These results show that the Fe-phthalocyanine dimer has the potential to design future molecular spintronic devices.

PACS: 73.23.−b, 85.65.+h DOI: 10.1088/0256-307X/34/4/047302

The rapid development of experimental techniques and theoretical methods allows us to predict and even build molecular devices with different functionalities. Most of the important physical effects in traditional silicon-based devices have been realized in molecular devices.[1−8] Recently, molecular spintronic devices have attracted great attention.[9] The utilization of the spin degree of freedom can help us to realize high-density information storage and high-speed data processing with low power consumption.[10] A number of novel physical properties, such as spin filtering,[11,12] magnetoresistance,[13,14] spin current rectification,[15,16] spin negative resistance (NDR),[17,18] have been found in various molecular spintronic devices. An important routine to build molecular spintronic devices is to adopt a magnetic molecule sandwiched between two nonmagnetic electrodes.[9,19] Among the multitudinous magnetic molecules, transition metal-coordination complexes form a promising and important family since their magnetic characteristics can be effectively tuned by introducing different transition metal atoms.[20]

The phthalocyanine (Pc) molecule has a large cavity which can accommodate various transition metal atoms.[21,22] In particular, the magnetic characteristics and magnetic transport properties of Fe-Pc have been investigated before. For example, Gao *et al.* found an unusually high Kondo temperature in Fe-Pc adsorbed on the Au(111) surface.[23] Deng *et al.* reported that the magnetic transport properties of Fe-Pc with Au electrodes can be effectively modulated by carbon chains with different connection sites.[24] In 2004, Makhseed *et al.* synthesized the dioxane-linked planar Pc dimer, which has two cavities to hold transition metal atoms.[25] In the present work, we explore the magnetic transport of the Fe-Pc dimer, which covalently bridges with two armchair single-walled carbon nanotube (ASWCNT(4,4)) electrodes.[26] The results show that the device can present high-performance spin filtering, magnetoresistance, and low-bias spin NDR effects by modulating the external magnetic field.

The geometric structure of the Fe-Pc dimer-based spintronic device is shown in Fig. 1, which is divided into three regions: left/right electrode (LE/RE) and central scattering region (CSR). The CSR includes the Fe-Pc dimer and 12 layers of carbon atoms from each electrode, which account for the molecule–electrode coupling and electrode screening effect. Both the LE and RE are depicted by a supercell with 3 repeated carbon unit cells along the z-direction. Since the intermetallic distance ($\sim$20 Å) is far for the spins to be coupled, the parallel (P) and antiparallel (AP) magnetic configurations (MCs) between the spin directions of two Fe atoms can be realized by tuning the external magnetic field.[27,28] The magnetic transport is calculated by using the ATOMISTIX TOOLKIT (ATK) package,[29,30] which is based on the spin-polarized density functional theory (DFT) combined with the non-equilibrium Green's function (NEGF) method. The local spin density approximation plus Hubbard U (LSDA+U) is used to describe the exchange-correlation potential.[31] For the $3d$ orbitals of Fe, we set the Hubbard U to a typical value of 4.0 eV.[32,33] The Troullier–Martins norm-conserving pseudo-potentials[34] and the linear combinations of local atomic orbitals in the double-zeta plus polarization (DZP) basis set are adopted for the core and valence electrons, respectively. The k-point sampling $1 \times 1 \times 100$ and 150 Ry for cutoff energy are used. Moreover, a large vacuum slab in the x- (20 Å) and y-direction (40 Å) is chosen to eliminate the interactions with neighboring periodic images. Before the transport calculations, the structure of CSR is fully relaxed until the atomic forces are converged below 0.02 eV/Å. The spin-polarized current through the device is computed by the Landauer–Büttiker formula[35] $I_\sigma(V) = (e/h)\int T_\sigma(E,V)[f_{\rm L}(E-\mu_{\rm L}) - f_{\rm R}(E-\mu_{\rm R})]dE$,where e and h are the elementary electron charge and Planck's constant, σ is the spin index with σ=up and

*Supported by the National Natural Science Foundation of China under Grant No 11104115, and the Natural Science Foundation of Shandong Province under Grant No ZR2016AM11.
**Corresponding author. Email: ss_zhaop@ujn.edu.cn; zhaopeng_sdu@sohu.com
© 2017 Chinese Physical Society and IOP Publishing Ltd

σ=dn for spin-up and spin-down, respectively, $f_{\mathrm{L(R)}}$ is the Fermi–Dirac distribution function, $\mu_{\mathrm{L(R)}} = E_{\mathrm{F}} \pm eV/2$ is the electrochemical potential of LE and RE, E_{F} is the Fermi level, which has been shifted to the energy origin for simplicity in our calculations, and $T_\sigma(E,V)$ is the spin-dependent transmission function and the spin-polarized current is thus determined by the integral of $T_\sigma(E,V)$ over the energy range, $[-eV/2, +eV/2]$, which is referred to as the energy bias window (EBW).

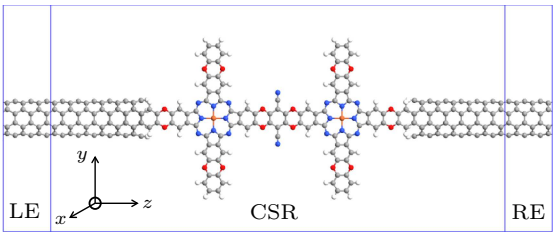

Fig. 1. Schematic view of the Fe-Pc dimer-based device, in which the Fe-Pc dimer covalently bridges two ASWCNT(4,4) electrodes. The LE, RE and CSR correspond to the left electrode, right electrode and central scattering region, respectively. The gray, blue, red, white and brown spheres represent C, N, O, H and Fe atoms, respectively.

The spin-resolved current–voltage (I–V) characteristics for P and AP MCs are presented in Fig. 2(a). The inset of Fig. 2(a) shows the I–V curves with bias greater than 0.15 V at a smaller scale. For the P MC, as the bias increases, the spin-down current I_{dn} increases rapidly at first and reaches its maximum at 0.05 V, and then decreases quickly, and beyond 0.15 V. Here I_{dn} becomes very small but it is still larger than zero, as shown in the inset of Fig. 2(a). In contrast, the spin-up current I_{up} is almost zero in the whole bias range. Therefore, the device under the P MC gives a nearly perfect spin filtering effect, which can be evaluated qualitatively by the ∼100% spin filtering efficiency (SFE=$[(I_{\mathrm{up}} - I_{\mathrm{dn}})/(I_{\mathrm{up}} + I_{\mathrm{dn}})] \times 100\%$), as shown in Fig. 2(b). Meanwhile, I_{dn} exhibits an obvious low-bias (0.05 V) spin NDR behavior, which is in favor of designing low-power consumption NDR-based devices.[4] For the AP MC, as shown in Fig. 2(a), both I_{up} and I_{dn} are dramatically inhibited. Thus the total current ($I_{\mathrm{up}}+I_{\mathrm{dn}}$) under the P MC ($I_{\mathrm{P}}$) is much larger than that under the AP MC (I_{AP}), and then a high-performance magnetoresistance effect can be obtained by switching the MC between P and AP. The magnetoresistance behavior can be further quantified by the magnetoresistance ratio (MR=$[(I_{\mathrm{P}} - I_{\mathrm{AP}})/I_{\mathrm{AP}}] \times 100\%$). As shown in Fig. 2(c), the MR is higher than $10^3\%$ when the bias is smaller than 0.3 V, and reaches its maximum $9.12 \times 10^5\%$ at 0.05 V, which is much larger than those reported previously.[36,37] Note that the SFE and MR are calculated by using the corresponding zero-bias transmission coefficient at E_{F} at zero bias, when all the currents vanish.

According to the Landauer–Büttiker formula, the device's current is the integral of the total transmission integral within the EBW. Hence, to explain the spin-dependent transport behaviors, the spin-resolved transmission spectra as functions of the electron energy E and bias V are plotted in Fig. 3, where the region between two dotted red lines is the EBW. Figures 3(a) and 3(b) correspond to the spin-up and spin-down transmission spectra under the P MC, while Figs. 3(c) and 3(d) correspond to the spin-up and spin-down transmission spectra under the AP MC, respectively. Evidently, for the P MC, there is no obvious spin-up transmission within the EBW (Fig. 3(a)), leading to the I_{up} under the P MC being negligible. In contrast, there are significant spin-down transmissions around E_{F} at low biases (Fig. 3(b)), which contribute the initial increase of I_{dn} and then the nearly perfect spin filtering effect under the P MC. As the bias increases (>0.15 V), those spin-down transmissions attenuate quickly beyond recognition, resulting in the rapid reduction of I_{dn} and thus the spin NDR effect occurs. For the AP MC, as shown in Figs. 3(c) and 3(d), it is clear that there is no spin-up and spin-down transmission within the EBW. As a result, both I_{up} and I_{dn} are strongly suppressed.

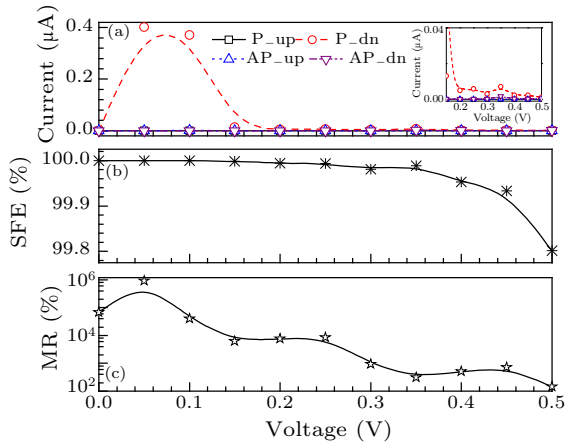

Fig. 2. (a) The spin-polarized I–V curves of P and AP MCs. The inset shows the I–V curves with bias greater than 0.15 V at a smaller scale. (b) The spin filtering efficiency (SFE) curves of P MC at various biases. (c) The magnetoresistance ratio (MR) as a function of applied bias.

The different transmission characteristics under different MCs and their evolution with the increase of bias can be understood by the bias-dependent energy levels of the molecular projected self-consistent Hamiltonian (MPSH) orbitals (Fig. 4), which have been modified by the electrodes,[38] as well as their spatial distributions (Fig. 5). Figures 4(a) and 4(b) correspond to the bias-dependent spin-up and spin-down energy levels under the P MC, while Figs. 4(c) and 4(d) correspond to the bias-dependent spin-up and spin-down energy levels under the AP MC, respectively. As shown in Figs. 4(a) and 4(b), there is only one spin-up MPSH orbital (331) entering into the EBW after 0.45 V, while there are five spin-down MPSH orbitals (332–336) within the EBW. As shown in Figs. 4(c) and 4(d), there are two (335 and 336) and three (336–338) most important MPSH orbitals within the EBW. Taking the cases of spin-down under the P MC and spin-up under the AP MC as exam-

ples, as shown in Fig. 5, we plot the spatial distributions of the most important MPSH orbitals within the EBW at 0.05 and 0.5 V, respectively. From the corresponding spatial distribution, we can see that both the spin-down MPSH orbitals 333 and 334 around E_F are delocalized at 0.05 V, indicating that they are good electron transport channels which lead to the obvious transmissions at low biases. With the increase of bias, for example, at 0.5 V, the delocalization degree of these two orbitals reduces significantly, and they become strongly localized on the left Fe-Pc parts, which block the electron transport and account for the vanishing of transmission at the corresponding energies. Moreover, 335 is also a strongly localized orbital (not shown here), and has no contribution for the electron transport. Orbitals 332 and 336 are localized to a certain extent (not shown here), which can only give rise to two very weak transmissions along the boundaries of the EBW (Fig. 3(b)). Therefore, I_{dn} under the P MC increases at low biases, and then decreases rapidly with the increase of bias, giving rise to the nearly perfect spin filtering and spin NDR effects. In contrast, the spin-up MPSH orbitals 335 and 336 under the AP MC at 0.05 and 0.5 V are completely localized on the right Fe-Pc parts. As a consequence, there is no observable transmission within the EBW (Fig. 4(c)). The cases of spin-up under the P MC and spin-down under the AP MC can be explained similarly (not shown here).

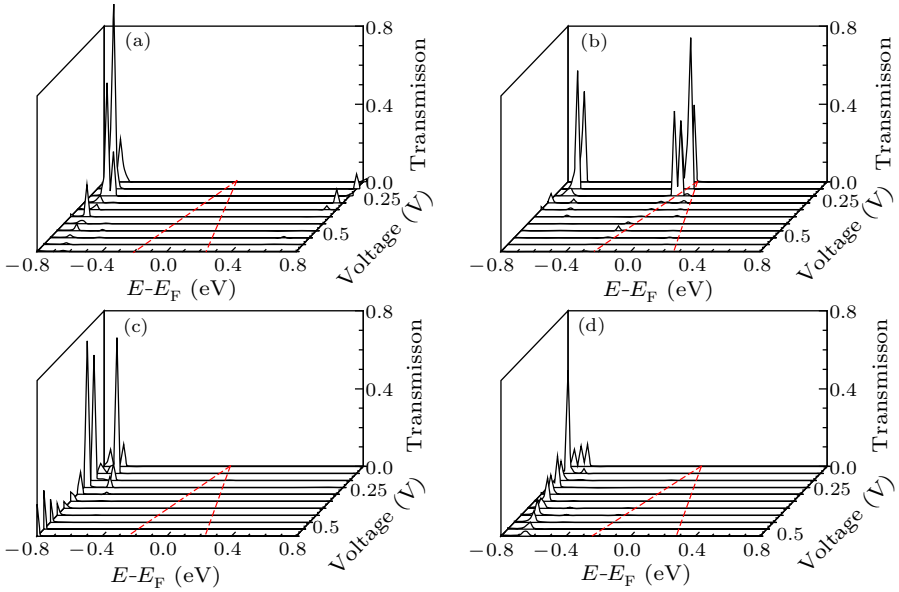

Fig. 3. The spin-resolved transmission spectra as functions of the electron energy E and bias V, where the region between two dotted red lines indicates the energy bias window (EBW). (a, b) The spin-up and spin-down transmission spectra under the P MC, and (c, d) the spin-up and spin-down transmission spectra under the AP MC, respectively. The Fermi level E_F has been shifted to the energy origin.

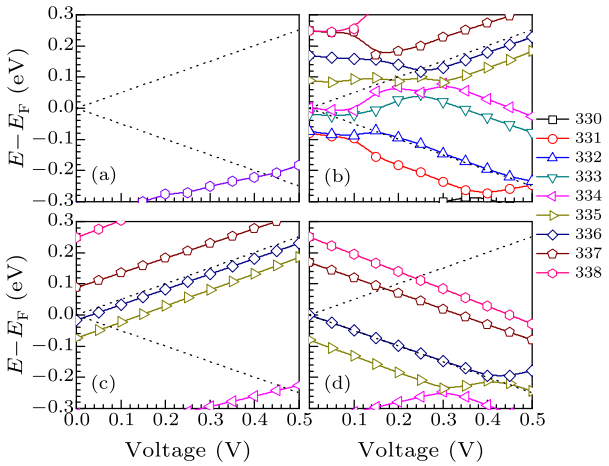

Fig. 4. The bias-dependent energy levels of the molecular projected self-consistent Hamiltonian (MPSH) orbitals. (a, b) The bias-dependent spin-up and spin-down energy levels under the P MC, and (c, d) the bias-dependent spin-up and spin-down energy levels under the AP MC, respectively.

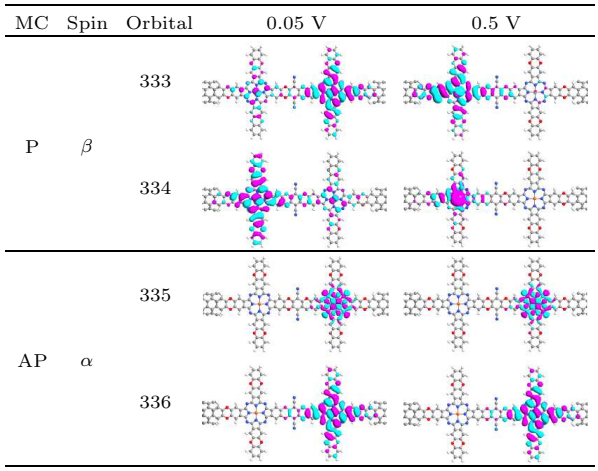

Fig. 5. The spatial distribution of the spin-down MPSH orbitals of 333 and 334 and spin-up MPSH orbitals of 335 and 336 under the P and AP MCs, respectively.

In summary, using the DFT+NEGF method, we have explored the magnetic transport of Fe-Pc dimer

with ASWCNT electrodes. The results show that the system can present high-performance spin filtering, magnetoresistance, and low-bias spin NDR effects by tuning the external magnetic field. The present findings could be helpful for the applications of Fe-Pc dimers in the field of molecular spintronic devices.

References

[1] Capozzi B, Xia J L, Adak O, Dell E J, Liu Z F, Taylor J C, Neaton J B, Campos L M and Venkataraman L 2015 *Nat. Nanotechnol.* **10** 522
[2] Zhang G P, Hu G C, Li Z L and Wang C K 2012 *J. Phys. Chem.* C **116** 3773
[3] Chen J, Reed M A, Rawlett A M and Tour J M 1999 *Science* **286** 1550
[4] Zhao P, Liu D S, Zhang Y, Su Y, Liu H Y, Li S J and Chen G 2012 *J. Phys. Chem.* C **116** 7968
[5] Fan Z Q, Zhang Z H, Deng X Q, Tang G P, Yang C H, Sun L and Zhu H L 2016 *Carbon* **98** 179
[6] Wu Q H, Zhao P and Liu D S 2014 *Chin. Phys. Lett.* **31** 057304
[7] Jiang X W and Li S S 2014 *Appl. Phys. Lett.* **104** 193510
[8] Li L, Engel M, Farmer D B, Han S and Philip W H S 2016 *ACS Nano* **10** 4672
[9] Bogani L and Wernsdorfer W 2008 *Nat. Mater.* **7** 179
[10] Ferrer J and García-Suárez 2009 *J. Mater. Chem.* **19** 1696
[11] Deng X Q, Zhang Z H, Tang G P, Fan Z Q, Sun L, Li C X and Zhang H L 2016 *Org. Electron.* **37** 245
[12] Zeng J, Chen K Q and Long M Q 2016 *Org. Electron.* **35** 12
[13] Bai J, Cheng R, Xiu F, Liao L, Wang M, Shailos A, Wang K L, Huang Y and Duan X 2010 *Nat. Nanotechnol.* **5** 655
[14] Wu Q H, Zhao P and Chen G 2015 *Org. Electron.* **25** 308
[15] Hu G C, Zhang Z, Zhang G P, Ren J F and Wang C K 2016 *Org. Electron.* **37** 485
[16] Deng X Q, Zhang Z H, Fan Z Q, Tang G P, Sun L and Li C X 2016 *Org. Electron.* **32** 41
[17] Jiang C, Wang X F and Zhai M X 2014 *Carbon* **68** 406
[18] Wu Q H, Zhao P and Liu D S 2016 *RSC Adv.* **6** 16634
[19] Wu Q H, Zhao P, Su Y, Li S J, Guo J H and Chen G 2015 *RSC Adv.* **5** 52938
[20] Sproules S and Wieghardt K 2010 *Cood. Chem. Rev.* **254** 1358
[21] Shen X, Sun L L, Yi Z L, Benassi E, Zhang R X, Shen Z Y, Sanvito S and Hou S M 2010 *Phys. Chem. Chem. Phys.* **12** 10805
[22] Zhou Y H, Zeng J, Tang L M, Chen K Q and Hu W P 2013 *Org. Electron.* **14** 2940
[23] Gao L, Ji W, Hu Y B, Cheng Z H, Deng Z T, Liu Q, Jiang N, Lin X, Guo W, Du S X, Hofer W A, Xie X C and Gao H J 2007 *Phys. Rev. Lett.* **99** 106402
[24] Deng X Q, Zhang Z H, Tang G P, Fang Z Q, Sun L and Li C X 2016 *Org. Electron.* **35** 1
[25] Makhseed S, Bumajdad A, Ghanem B, Msayib K and McKeown N B 2004 *Tetrahedron Lett.* **45** 4865
[26] Huang J, Wang W Y, Yang S F, Su H B, Li Q X and Yang J L 2012 *Chem. Phys. Lett.* **539** 102
[27] Zeng J and Chen K Q 2014 *Appl. Phys. Lett.* **104** 033104
[28] Zeng J and Chen K Q 2015 *J. Mater. Chem.* C **3** 5697
[29] Taylor J, Guo H and Wang J 2001 *Phys. Rev.* B **63** 245407
[30] Brandbyge M, Mozos J L, Ordejón P, Taylor J and Stokbro K 2002 *Phys. Rev.* B **65** 165401
[31] Anisimov V I, Solovyev I V and Korotin M A 1993 *Phys. Rev.* B **48** 16929
[32] Rai D P, Shankar A, Sandeep, Ghimire M P and Thapa R K 2012 *Physica* B **407** 3689
[33] Jin L and Zhou C 2013 *Prog. Nat. Sci.-Mater.* **23** 413
[34] Troullier N and Martins J 1991 *Phys. Rev.* B **43** 1993
[35] Büttiker M and Landauer R 1985 *Phys. Rev.* B **31** 6207
[36] Zeng J and Chen K Q 2016 *Carbon* **104** 20
[37] Wu Q H, Zhao P, Liu D S and Chen G 2013 *Solid State Commun.* **174** 5
[38] Stokbro K, Taylor J, Brandbyge M, Mozos J L and Ordejón P 2003 *Comput. Mater. Sci.* **27** 151